Development 134, 921-931 (2007) doi:10.1242/dev.02776

New functions for a vertebrate Rho guanine nucleotide exchange factor in ciliated epithelia

Jennifer R. Panizzi[1], Jason R. Jessen[2], Iain A. Drummond[3] and Lilianna Solnica-Krezel[1,*]

Human ARHGEF11, a PDZ-domain-containing Rho guanine nucleotide exchange factor (RhoGEF), has been studied primarily in tissue culture, where it exhibits transforming ability, associates with and modulates the actin cytoskeleton, regulates neurite outgrowth, and mediates activation of Rho in response to stimulation by activated Gα12/13 or Plexin B1. The fruit fly homolog, RhoGEF2, interacts with heterotrimeric G protein subunits to activate Rho, associates with microtubules, and is required during gastrulation for cell shape changes that mediate epithelial folding. Here, we report functional characterization of a zebrafish homolog of ARHGEF11 that is expressed ubiquitously at blastula and gastrula stages and is enriched in neural tissues and the pronephros during later embryogenesis. Similar to its human homolog, zebrafish Arhgef11 stimulated actin stress fiber formation in cultured cells, whereas overexpression in the embryo of either the zebrafish or human protein impaired gastrulation movements. Loss-of-function experiments utilizing a chromosomal deletion that encompasses the *arhgef11* locus, and antisense morpholino oligonucleotides designed to block either translation or splicing, produced embryos with ventrally-curved axes and a number of other phenotypes associated with ciliated epithelia. Arhgef11-deficient embryos often exhibited altered expression of laterality markers, enlarged brain ventricles, kidney cysts, and an excess number of otoliths in the otic vesicles. Although cilia formed and were motile in these embryos, polarized distribution of F-actin and Na^+/K^+-ATPase in the pronephric ducts was disturbed. Our studies in zebrafish embryos have identified new, essential roles for this RhoGEF in ciliated epithelia during vertebrate development.

KEY WORDS: Pronephros, Left-right asymmetry, Otoliths, PDZ-RhoGEF, Arhgef11, Cell polarity, Zebrafish

INTRODUCTION

Rho guanine nucleotide exchange factors (RhoGEFs) are specialized proteins that directly bind to and activate Rho family GTPases in response to upstream regulatory signals, thus linking extracellular signals with intracellular responses. At least 70 RhoGEFs have been identified in the human genome, many of which have homologs in other vertebrate and invertebrate species (Schmidt and Hall, 2002; Rossman et al., 2005). Most of these RhoGEFs possess both Dbl-homology (DH) and Pleckstrin-homology (PH) domains in tandem. These domains often interact specifically with the target GTPase(s) and constitute the functional nucleotide exchange subunit (Cerione and Zheng, 1996). In addition to the DH and PH domains, many RhoGEFs possess domains that modulate their functions and connect Rho to a variety of signaling pathways. The regulator of G protein-coupled signaling (RGS) domains link G protein-coupled signaling to Rho by binding the alpha subunits of activated heterotrimeric G proteins to RhoGEFs. The family of RGS-domain-containing RhoGEFs includes ARHGEF1 (p115RhoGEF), ARHGEF12 (Leukemia Associated RhoGEF, LARG) and ARHGEF11 (KIAA0380, PDZ-RhoGEF) (Fukuhara et al., 2001). Both ARHGEF11 and ARHGEF12 also contain a PDZ (PSD-95/DLG/ZO1) domain, which has been shown to interact with the C-terminus of the Semaphorin receptor, Plexin B1 (Swiercz et al., 2002). Through this interaction, Semaphorin 4D stimulation of Plexin B1 activates Rho signaling pathways and influences axon guidance (Aurandt et al., 2002; Perrot et al., 2002; Swiercz et al., 2002). These studies demonstrate that activation of Rho via ARHGEF11 and ARHGEF12 can be modulated through both the PDZ and RGS domains.

Thus far, human ARHGEF11 and its closely related family member, ARHGEF12, have been studied primarily in cell culture, where they activate Rho and promote reorganization of the actin cytoskeleton in response to stimulation by heterotrimeric G protein subunits Gα12/13 (Fukuhara et al., 1999). In addition to the work illuminating the interactions and roles of the conserved domains of ARHGEF11, further studies have delineated other regions of the protein that may be important for its function. One such region is the C-terminus, which may interact with p-21 activated kinase 4 (PAK4), or homo- or heterodimerize with the C-terminus of another ARHGEF11 or ARHGEF12 molecule (Barac et al., 2004; Chikumi et al., 2004). Moreover, a small region of ARHGEF11 between the RGS and DH domains has been shown to interact with the actin cytoskeleton (Banerjee and Wedegaertner, 2004). These reported interactions and functions were determined using yeast and mammalian cell culture systems, where both ARHGEF11 and ARHGEF12 exhibit very similar activities. Interestingly, there is evidence from mouse studies suggesting that the expression profiles of these two proteins are somewhat different, with ARHGEF11 detected predominantly in neural tissues and ARHGEF12 found in both neural and non-neural tissues (Kuner et al., 2002). Therefore, although ARHGEF11 and ARHGEF12 seem to have mostly redundant activities in cultured cells, these functions may be modulated differently and in a tissue-specific manner.

Most of our knowledge of in vivo roles for ARHGEF11 has come from work conducted with the fruit fly homolog, RhoGEF2, which contains all the major domains and displays significant sequence similarity with ARHGEF11. RhoGEF2 was first identified in a screen for Rho signaling pathway components, and was further shown to

[1]Department of Biological Sciences, Vanderbilt University, Nashville, TN 37235, USA. [2]Department of Medicine, Vanderbilt University Medical School, Nashville, TN 37232, USA. [3]Nephrology Division, Harvard Medical School, Massachusetts General Hospital, Charlestown, MA 02129, USA.

*Author for correspondence (e-mail: lilianna.solnica-krezel@vanderbilt.edu)

Accepted 6 December 2006

control cell shape changes during gastrulation (Barrett et al., 1997; Hacker and Perrimon, 1998). This RhoGEF also associates with microtubules via the plus-end-binding protein, EB1, and regulates actomyosin contraction in the epithelia of the developing embryo (Rogers et al., 2004; Padash Barmchi et al., 2005). Additionally, apical distribution of RhoGEF2 and other Rho activators together with the basolateral distribution of Rho inhibitors are required to modulate actin via Rho during cell invagination and lumen formation for proper development of the spiracle in the fruit fly (Simoes et al., 2006).

Studies of these vertebrate and invertebrate PDZ-domain-containing RhoGEFs suggest they may act similarly to regulate the cytoskeleton by modulating Rho in response to G protein-coupled signaling, possibly while associating with actin and/or microtubules. Despite all the information garnered from cultured cells and the *D. melanogaster* system, the roles of ARHGEF11 in developing and adult vertebrates remain to be elucidated.

Here we use the zebrafish model, which is particularly amenable to in vivo analysis, to assess the functions of a zebrafish homolog of human ARHGEF11 during vertebrate development. Employing several loss-of-function approaches, we have identified new and unanticipated roles for this vertebrate RhoGEF in processes involving ciliated epithelia, including establishment of left-right asymmetry, formation of otoliths in the otic vesicle, and development of the pronephros.

MATERIALS AND METHODS

Zebrafish maintenance, embryo generation and staging

Wild-type (WT) zebrafish of AB, India, TL and hybrid strains were maintained as previously described (Solnica-Krezel et al., 1994). Embryos were obtained from natural matings and staged according to morphology (Kimmel et al., 1995).

Cloning and sequencing of *arhgef11*

Positional cloning of the *trilobite* locus revealed *arhgef11* nearby on chromosome 7 (Jessen et al., 2002). Using 5′ and 3′ SMART RACE (BD Biosciences), partial UTR and the entire coding sequence of *arhgef11* were determined. Total RNA was isolated from 2- to 8-cell or 48-hour WT embryos using TRIzol Reagent (Invitrogen), and used to produce cDNA via the Superscript First-Strand Synthesis System (Invitrogen). Using primers to the 5′ (5′-CGGAATTCCGTCATGAATGTCCGACACC-3′ or 5′-CGGAATTCCACTACACTAATAACCGGACAAACC-3′) and 3′ (5′-GCTCTAGAAGCGTCAGAAACCAGTGGAC-3′) UTR, both the ‘early’ and ‘late’ splice variants of *arhgef11* were PCR-amplified from cDNA using Platinum Pfx DNA Polymerase (Invitrogen). The complete coding sequence was amplified and cloned into the *Eco*RI-*Xba*I sites of the pCS2+ vector (Rupp et al., 1994), then verified by sequencing. N-terminal-tagged *arhgef11* constructs were made by subcloning into myc-pCS2+.

RT-PCR was performed by isolating RNA and producing cDNA as described above from embryos at the indicated stages. The resultant cDNAs were used as templates to amplify small regions of the gene encompassing the alternatively-spliced exons.

The construct encoding the dominant-negative form of Arhgef11, *Δdhph*, was generated so as to lack the DH and PH domains by using the myc-tagged full-length ‘early’ construct as a template to amplify the protein-encoding regions directly 5′ and 3′ of the DH-PH tandem, while inserting an *Xho*I site in its place with the following primers: 5′-CGCTCGAGTAATATGTGCGGCTCCACTG-3′ and 5′-CGCTCGAGTCTGCCGATCAGTCAGAAGG-3′. This site was then used to ligate the fragments together without the DH and PH domains.

The *arhgef11* full-length gene sequence reported in this paper has been deposited in GenBank under the accession number AY295347.

In situ hybridization

Sense and antisense probes for *arhgef11* were made with digoxigenin-labeled NTPs (Roche) using pCS2-*arhgef11* constructs linearized with *Not*I or *Eco*RI as templates for RNA synthesis with SP6 or T7 RNA polymerases, respectively. Antisense probes for *southpaw* (*spaw*) (Long et al., 2003), *pitx2* (Tsukui et al., 1999), *cardiac myosin light chain 2* (*cmlc2*; *myl7* – Zebrafish Information Network) (Yelon et al., 1999) and *preproinsulin* (*ins*) (Milewski et al., 1998) were prepared as described previously. Embryos were fixed at the stages indicated and processed essentially as previously described (Thisse and Thisse, 1998). Some of the stained embryos were embedded in a solution of 1.2% agarose, 30% sucrose and cryosectioned using a Leica CM1900.

RNA and morpholino injections

Capped sense RNA encoding Arhgef11 was synthesized with SP6 RNA polymerase (Ambion mMessage mMachine system) after linearization of the pCS2-*arhgef11* construct with *Not*I. RNA was purified using G-50 Sephadex Quick Spin Columns (Roche) and diluted with tissue culture grade distilled water. Microinjections into 1- to 4-cell embryos were performed as described previously (Marlow et al., 1998).

A translation-blocking morpholino oligonucleotide (MO), MO^{AUG} (Gene-Tools, LLC), targeted to the 5′-UTR (5′-GACGGAGGTTTGTCCGGTTATTAGT-3′) and a splice-blocking MO, MO^{SPL} (Open Biosystems), targeted to the exon 10-intron 10 boundary (5′-GGATACACTCACCTCCACGTCTCCT-3′) were used. MOs were diluted and microinjected as described above.

Stress fiber formation assay

HEK293 cells were grown to confluence in DMEM supplemented with 10% FBS, 1× penicillin/streptomycin and 2 mM GlutaMAX (Gibco), then plated onto poly-D-lysine (Sigma) -coated coverslips in 6-well plates at 4×10^5 cells per well. After reaching 50-70% confluence, cells were transfected with myc-pCS2 containing *arhgef11* or *Δdhph*, or pCS2-GFP as a control, using *Trans*IT-LT1 Transfection Reagent (Mirus). After 24 hours, cells were serum-starved for 4 hours. As a positive control, 10 nM thrombin (a gift from P. E. Bock, Vanderbilt University Medical School, Nashville, TN) was then added for 20 minutes. After fixation with 4% paraformaldehyde (PFA) in PBS, cells were immunostained using AlexaFluor546-phalloidin (Molecular Probes) and Rabbit anti-c-myc (Research Diagnostics) with Cy2-anti-Rabbit (Jackson ImmunoResearch Laboratories) antibodies, then visualized by confocal microscopy (Zeiss LSM510 META). The GFP construct used as transfection control was made by subcloning GFP coding sequence from the pEGFP-N1 vector (Clontech) into pCS2+.

Antibody production

A portion of the ‘early’ *arhgef11* construct encoding amino acids 509-736 was amplified and cloned into a pET30a+ vector (Novagen). The construct was expressed and purified essentially as described previously (Panizzi et al., 2006). The fragment was dialyzed into PBS, then sent to ProSci for rabbit polyclonal antibody production.

Western blotting

Zebrafish embryos were manually dechorionated and deyolked before lyzing. Laemmli SDS reducing sample buffer (Laemmli, 1970) was added to the lyzate before loading onto 4-15% Tris-HCl Ready Gels (BioRad) and electrophoresis in Tris-glycine-SDS buffer (Laemmli, 1970). Proteins were then transferred to Immobilon-P membrane (Millipore) in Tris-glycine buffer and the membranes processed essentially as described previously (Iwamoto et al., 2006), using the primary antibodies indicated.

Immunohistochemistry

Embryos were grown to the indicated stages and processed essentially as described previously (Topczewska et al., 2001), using CY2-, CY5- or CY3-conjugated secondary antibodies (Jackson ImmunoResearch Laboratories). Where indicated, AlexaFluor546-phalloidin was added with secondary antibody to visualize F-actin. Embryos were analyzed by confocal microscopy (Zeiss LSM510 META).

Antibody staining on cryosections was performed essentially as described above, except that Tween 20 was omitted and that PBS containing 5% evaporated milk, 5% goat serum was used for blocking. For Na^+/K^+-ATPase detection, fixation was performed overnight at –20°C in Dent’s fixative (80% methanol, 20% DMSO).

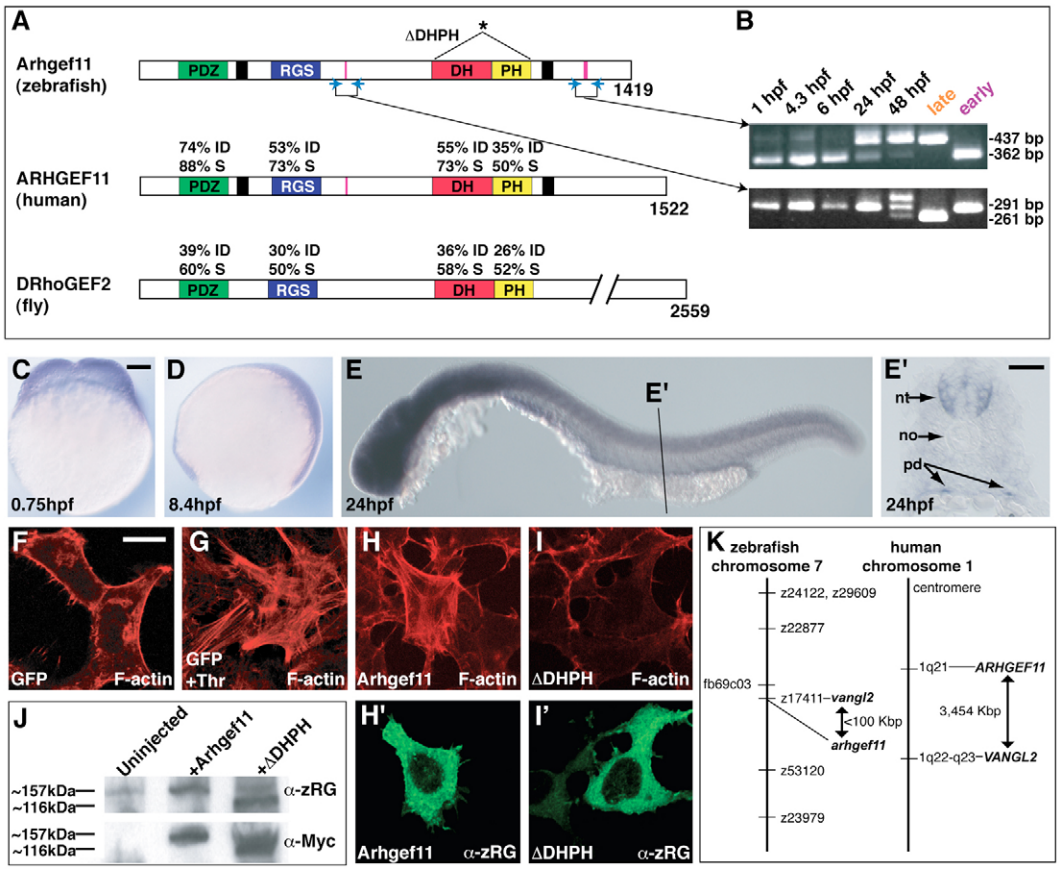

Fig. 1. Zebrafish Arhgef11 is a homolog of human ARHGEF11 and is expressed during early embryogenesis. (**A**) Schematic depicting the percentage of identical (I) and similar (S) amino acids between known functional domains of zebrafish Arhgef11 and its human and fly homologs. An asterisk marks the domains omitted in the dominant-negative construct (ΔDHPH). (**B**) Ethidium bromide stained agarose gel showing RT-PCR products after amplification of the indicated fragments (blue arrows in A) at the listed developmental times, along with fragments amplified from 'early' and 'late' cloned constructs. Alternatively-spliced exons are indicated by pink bars in A. (**C-E**) WT embryos after whole-mount in situ hybridization using antisense probe for *arhgef11* at the indicated developmental stages. Scale bar, 100 μm. (**E'**) Cryosection through the indicated region in E. Abbreviations: nt, neural tube, no, notochord, pd, pronephric ducts. Scale bar, 50 μm. (**F-I'**) Serum-starved cultured HEK293 cells expressing GFP, myc-Arhgef11, or myc-ΔDHPH. Cells in G were incubated with thrombin. F-actin is visualized by phalloidin in red (F-I), and Arhgef11 or ΔDHPH constructs are in green (H' and I', respectively) as detected by α-zRG. Scale bar, 20 μm. (**J**) Western blots using protein extracts from 6 hpf WT embryos injected as indicated. α-zRG detects both endogenous and overexpressed forms of full-length Arhgef11 (~157 kDa) and overexpressed ΔDHPH (~116 kDa), whereas α-Myc only detects the overexpressed forms of each. (**K**) Schematics of chromosomal locations of zebrafish and human *arhgef11* genes, showing synteny between the two chromosomes in the region encompassing *arhgef11*.

In addition to anti-zRG, the following primary antibodies were used: α6F (anti-Na^+/K^+-ATPase; Developmental Studies Hybridoma Bank), anti-aPKCζ (Santa Cruz Biotechnology), anti-ZO1 (Zymed Laboratories), anti-γ-tubulin and anti-acetylated tubulin (Sigma).

Histological sections

Embryos fixed in 4% PFA in PBS were dehydrated with ethanol and embedded in JB-4 resin (Polysciences) as described in the manufacturer's protocol. Using the Leica RM2265, ~4 μm sections were obtained, and then processed with hematoxylin and eosin (BBC Biochemical) according to the manufacturer's protocol.

Live imaging of cilia

Movies were captured and processed as described previously (Kramer-Zucker et al., 2005).

RESULTS

Two forms of zebrafish *arhgef11* are expressed during early embryogenesis

In our search for genes involved in early embryonic development, we identified a zebrafish PDZ-domain-containing RhoGEF gene linked to the *trilobite/vangl2* locus on chromosome 7 (Jessen et al., 2002). Sequence analysis by BLAST (Tatusova and Madden, 1999) revealed that this gene encodes a protein of 1419 amino acids that shares 40% identity and a further 13% similarity with human ARHGEF11 (Nagase et al., 1997; Fukuhara et al., 1999), and bears even higher similarity within each of the conserved domains (Fig. 1A). In addition, the zebrafish protein has significant similarity to RhoGEF2 from *D. melanogaster* (Barrett et al., 1997; Hacker and Perrimon, 1998), particularly within each of the conserved domains (Fig. 1A). Based on our analysis of the zebrafish genomic DNA sequence, we predict *arhgef11* comprises more than 40 small exons (data not shown), much like its human counterpart (Hubbard et al., 2005). Interestingly, there is also conserved synteny between the region of zebrafish chromosome 7 containing *arhgef11* and *vangl2/trilobite* and the region of human chromosome 1 that contains their human homologs (Fig. 1K). The amino acid sequence similarity coupled with the syntenic relationship support the notion that *arhgef11* is the ortholog of human *ARHGEF11*, and the encoded proteins are likely to share many of the same functions.

To study the gene in the developing zebrafish embryo, we cloned two *arhgef11* isoforms using cDNA synthesized from the RNA of embryos at 2 days post-fertilization (dpf). Both cloned forms of *arhgef11* contain the complete coding sequence for all four of the conserved domains, whereas small exons outside these regions are alternatively-spliced (Fig. 1A, pink bars). Further analysis by RT-PCR on embryos at stages from 1 hour post-fertilization (hpf) to 2 dpf demonstrated that these two isoforms are expressed dynamically during early embryogenesis (Fig. 1B). Sequence analysis of the first

isoform revealed that it lacks the exon encoding amino acids 1232-1257 of the predicted full-length transcript, situated near the C-terminus just after the PH domain (Fig. 1A). Furthermore, RT-PCR amplification of a small fragment using primers flanking this alternatively-spliced exon showed that this form persists from early cleavage stages through to 2 dpf, and we henceforth refer to it as the 'early' form (Fig. 1B). In addition, we identified another site of alternative splicing between the RGS and DH domains at the exon encoding amino acids 556-566 of the predicted full-length transcript (Fig. 1A). The form lacking this exon was only detected after 1 dpf (Fig. 1B), and is hereafter referred to as the 'late' form. Although these seem to be the most highly represented forms of *arhgef11* during early development, RT-PCR experiments indicated that the full-length form is also present (data not shown).

Arhgef11 induces actin stress fiber formation in cultured cells

We next assayed for functional similarities between the human and zebrafish forms of ARHGEF11 in cell culture. After serum starvation, cultured HEK293 cells transfected with human ARHGEF11 develop actin stress fibers as a result of RhoA stimulation (Rumenapp et al., 1999). We predicted that zebrafish Arhgef11 acts similarly owing to the conservation of crucial amino acids within the DH domain required for Rho specificity (see Fig. S1 in the supplementary material) (Oleksy et al., 2006). Accordingly, we found that after transfection of HEK293 cells with plasmid containing *myc-arhgef11 (early form)*, the protein was distributed throughout the cell with modest enrichment near the cell membrane (Fig. 1H′ and data not shown), and the cells developed actin stress fibers following serum starvation (Fig. 1H). Cells transfected with a GFP-containing plasmid (Fig. 1F) did not form actin stress fibers, serving as both a transfection and negative control. As a positive control, GFP-transfected cells were incubated with thrombin (Fig. 1G), a potent stimulator of actin stress fiber formation (Murphy et al., 2001).

In addition to the phenotypic similarities observed after overexpression of human or zebrafish Arhgef11 in cell culture, the effects they had on the developing zebrafish embryo were virtually indistinguishable. When either form was overexpressed by microinjection of synthetic RNAs, blastula stage embryos accumulated a large mass of cells within the blastoderm and failed to properly complete gastrulation movements (data not shown).

Spatiotemporal expression pattern of Arhgef11 RNA and protein during zebrafish development

To further understand the roles of this RhoGEF during vertebrate development, we used digoxigenin-labeled antisense probes to determine the localization of RNA encoding Arhgef11 by in situ hybridization in zebrafish embryos at different developmental stages. Transcripts were detected in each cell at early cleavage stages, less than 1 hpf and before zygotic transcription begins (Kane and Kimmel, 1993), indicating a maternal contribution of *arhgef11* (Fig. 1C). Embryos undergoing gastrulation movements, at just over 8 hpf, also expressed *arhgef11* ubiquitously (Fig. 1D). By 24 hpf, the transcripts became localized largely to the head, central nervous system and pronephric ducts (Fig. 1E,E′). No signal was detected when a digoxigenin-labeled sense probe for *arhgef11* was used (data not shown).

To gain insight into the function of Arhgef11 protein, we synthesized a peptide encoding amino acids 509-736, which are located between the RGS and DH domains, and developed a rabbit polyclonal antibody (α-zRG). We first tested the ability of this antibody to detect the myc-tagged full-length protein by western blotting. A band of the predicted molecular weight (~157 kDa) was detected in embryo extracts using either whole serum or affinity-purified antibody, but not with preimmune serum (Fig. 1J and data not shown). In extracts of embryos microinjected with synthetic RNA encoding a myc-tagged Arhgef11, the ~157 kDa band detected by α-zRG was more intense and was also detected by polyclonal antibodies for c-myc (Fig. 1J). We next tested the ability of the whole serum and the affinity-purified antibody to detect endogenous protein via whole-mount immunostaining of the zebrafish embryos. By this method, we were unable to detect significant amounts of Arhgef11 in cells of the early gastrula (6 hpf) or during early segmentation (13 hpf) (data not shown). However, at 24 hpf, fluorescent immunostaining was remarkably similar to the RNA expression data, revealing enrichment of Arhgef11 in the anterior region of the embryos and in cells lining the pronephric ducts (Fig. 6A and data not shown).

Loss-of-function studies uncover novel and essential developmental roles for Arhgef11

To assess the function of Arhgef11 in the developing zebrafish embryo, we employed four different loss-of-function strategies. First, we utilized an antisense morpholino oligonucleotide, MO^{AUG}, designed to block translation by binding to 25 bases of the 5′ UTR just upstream of the start codon (Nasevicius and Ekker, 2000). Whereas this type of interference does not affect maternally-deposited protein, it does inhibit production of new protein from both maternally-contributed and zygotically-produced RNA, making it a powerful tool for studying the effects of near-total loss of function during early stages of development. In fact, microinjection of 2-20 ng of MO^{AUG} per embryo led to marked dose-dependent developmental defects. The ability of MO^{AUG} to block the translation of endogenous Arhgef11 was tested by western blotting analysis on extracts from embryos microinjected with a moderate dose (4 ng) of the oligonucleotide. When compared with that of uninjected WT control embryo extracts, MO^{AUG}-injection yielded a dramatic reduction in Arhgef11 protein levels after 13 hpf, but produced no change in levels of an unidentified protein also recognized by the antibody (Fig. 2A). Interestingly, at least 85% of embryos injected with MO^{AUG} exhibited an abnormal ventrally-curved body shape and enlarged brain ventricles at 32 hpf (Fig. 2C), as compared with uninjected WT siblings (Fig. 2B). After 80 hpf, MO^{AUG}-injected embryos developed pericardial edema and severe distension of the pronephros (Fig. 6I). Most of these embryos did not survive past 4 dpf of development, suggesting that Arhgef11 function is crucial during these early developmental stages.

Since rescue attempts by co-injection with full-length RNA were impeded by the aforementioned gain-of-function phenotypes during gastrulation, we used a second MO to confirm that the observed morphant defects were due to loss of Arhgef11 function. This morpholino, MO^{SPL}, was designed to bind to the exon 10-intron 10 boundary and block splicing of the zygotically-synthesized *arhgef11* transcript (Fig. 2G). RT-PCR and sequencing analysis of RNA isolated from embryos injected with 5 ng MO^{SPL} confirmed that the resulting *arhgef11* RNA encodes a protein truncated just before the RGS domain as a result of a frameshift and premature stop codon after exclusion of exon 10 (Fig. 2H and data not shown). Moreover, the resulting embryos displayed phenotypes remarkably similar to those observed in embryos microinjected with MO^{AUG}, including the ventral body curvature (Fig. 2F). Whereas Arhgef11 levels at 13 hpf were modestly reduced in embryos injected with MO^{SPL} alone, co-injection of both MOs led to near-complete absence of this protein (Fig. 2I).

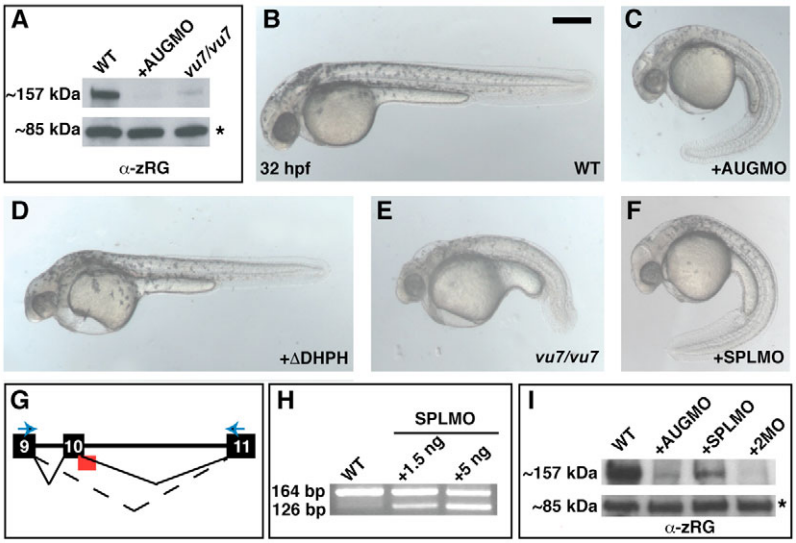

Fig. 2. Interference with Arhgef11 function yields morphological defects in zebrafish embryos. (**A**) Western blot using α-zRG on extracts prepared at 13 hpf from the indicated embryos. The asterisk marks expression of an unidentified 85 kDa protein also detected by α-zRG. (**B-F**) Live embryos at 32 hpf: uninjected WT (B), WT injected with 4 ng MO^{AUG} (AUGMO; C), WT injected with 350 pg of RNA encoding ΔDHPH construct (D), *vu7/vu7* mutants (E) and WT injected with 5 ng MO^{SPL} (SPLMO) (F). Scale bar, 300 μm. (**G**) Schematic depicting the MO^{SPL}-binding site (red) at the exon 10-intron 10 boundary, with normal (solid line) and disrupted (dotted line) splicing shown. (**H**) Ethidium bromide stained agarose gel of RT-PCR products amplified from embryos after the indicated treatment using the primers represented by the blue arrows in G. (**I**) Western blot using α-zRG on extracts prepared at 13 hpf from uninjected WT, or WT after injection with 4 ng MO^{AUG}, 5 ng MO^{SPL}, or co-injected with both.

In a parallel approach to study Arhgef11 loss-of-function, we employed a gamma-irradiation-induced deletion mutation, *vu7*, encompassing *arhgef11*, *vangl2/trilobite* and at least two other nearby genes (J.R.P., J.R.J. and L.S.-K., unpublished). Homozygous *vu7/vu7* mutant embryos, recognized by their shortened bodies resulting from loss of the *vangl2/trilobite* gene (Jessen et al., 2002), also showed a marked decrease in Arhgef11 protein levels at 13 hpf (Fig. 2A). Similar to the *arhgef11* morphants, these embryos had slight ventral body curvature, enlarged brain ventricles at 32 hpf, and developed pericardial edema and distension of the pronephros by 2 dpf (Fig. 2E and data not shown). However, owing to the deletion of genes other than *arhgef11* and *vangl2/trilobite*, these mutant embryos also exhibited additional phenotypes, including brain degeneration after 2 dpf, which we attribute to loss of an unidentified gene within the deletion (J. A. Clanton, J.R.P. and L.S.-K., unpublished). Additionally, as *vu7/vu7* mutant embryos are produced by heterozygous matings, maternally-contributed Arhgef11 protein and RNA account for a milder reduction of protein levels, and therefore milder phenotypes, than those observed in *arhgef11* morphants (Fig. 2A; Fig. 3E,J; Fig. 5C).

In our fourth strategy to assess Arhgef11 function, we generated a dominant-negative construct encoding a stable protein with a predicted molecular weight of 117 kDa that lacks the DH and PH domains (ΔDHPH) previously shown to be required for Rho activation (Fig. 1A,J). Notably, a similar construct has been reported to block G protein-coupled activation of RhoA in mammalian cell culture (Rumenapp et al., 1999). This construct presumably acts as a competitive inhibitor of the endogenous protein through its binding to upstream components and inability to activate Rho. Owing to the nature of this interference technique, it could also disrupt signaling of other PDZ- and RGS-domain-containing RhoGEFs such as Arhgef1 and Arhgef12. Expression of the ΔDHPH construct in HEK293 cells revealed that it neither localized to the cell membrane like its WT counterpart, nor induced formation of actin stress fibers (Fig. 1I,I′). Embryos injected with 350-700 pg of synthetic RNA encoding ΔDHPH exhibited dose-dependent developmental defects including a widened anterior body region, pericardial edema and frequent cardia bifida (Fig. 2D and data not shown). These defects could be suppressed by co-injection of the full-length construct (data not shown). Taken together, the data obtained from all these approaches indicate that Arhgef11 plays an essential role during zebrafish embryogenesis.

Arhgef11 function is important for establishment of left-right asymmetry

The curved body axis and pronephric cysts observed in Arhgef11 morphant embryos were similar to phenotypes observed in *inversin* and *polaris* (*ift88* – Zebrafish Information Network) morphant and mutant embryos, which display defects in left-right asymmetry and other cilia-mediated processes (Otto et al., 2003; Bisgrove et al., 2005; Kramer-Zucker et al., 2005). Left-right asymmetry is marked by sided gene expression that ultimately affects the orientation of many organs including the heart, pancreas, liver and certain regions of the brain (Levin, 2005). Kupffer's vesicle, a small epithelial structure comprising cells with motile cilia that create a directional fluid flow, has been shown to play a key role in the early steps of establishing the left-right axis (Essner et al., 2005; Kramer-Zucker et al., 2005). Given these phenotypic similarities, we examined the effect of loss of Arhgef11 function on left-right asymmetry.

First, we analyzed WT embryos injected with MO^{AUG}, MO^{SPL}, or the *Δdhph* construct, and *vu7/vu7* mutants using in situ hybridization with antisense probes for the asymmetrically-expressed genes *spaw* and *pitx2* (Tsukui et al., 1999; Long et al., 2003). *spaw* RNA, encoding a Nodal-related protein, was detected in the left lateral plate mesoderm (LPM) at ~19 hpf in most uninjected WT embryos, whereas this expression was somewhat randomized or absent in *vu7/vu7* embryos and in WT injected with MO^{AUG}, MO^{SPL} or *Δdhph* (Fig. 3A-E; Table 1). Expression of *pitx2* RNA, encoding a Bicoid-related transcription factor, was also disrupted in the LPM of Arhgef11-deficient embryos at 21 hpf (Fig. 3E-I; Table 1). Whereas most uninjected WT embryos had normal left-sided expression, embryos in which Arhgef11 function was disturbed exhibited not only left-sided but also bilateral, right-sided, and absent expression in the LPM. By contrast, the expression of *pitx2* in Rohon Beard cells was not affected in any of these loss-of-function experiments (arrowheads in Fig. 3F-I).

Finally, we analyzed localization of the heart and pancreas, two organs that are asymmetrically located, after 30 hpf or 53 hpf, respectively. We probed for *cmlc2* RNA (Yelon et al., 1999) to visualize the heart and *ins* (Milewski et al., 1998) to mark the

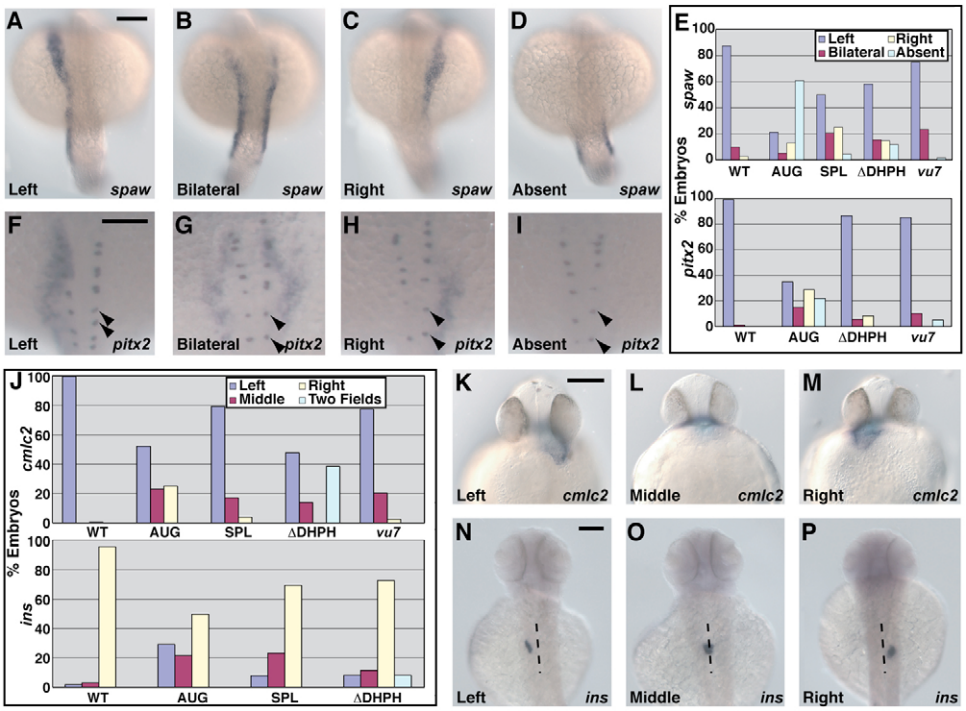

Fig. 3. Loss of Arhgef11 function leads to abnormal expression of laterality markers. (**A-D**) Expression of *spaw* in 19- to 22-somite stage (~19 hpf) embryos detected by in situ hybridization with antisense RNA probe. Scale bar, 150 μm. (**E**) Bar graph of the percentage of WT and treated embryos exhibiting the expression patterns for *spaw* shown in A-D, or *pitx2* shown in F-I. (**F-I**) Expression of *pitx2* in 22- to 25-somite stage (~21 hpf) embryos detected by in situ hybridization with antisense RNA probe. Expression of *pitx2* in Rohon Beard cells (marked by arrowheads) is not disrupted. Scale bar, 150 μm. (**J**) Graphical representation of the percentage of embryos exhibiting the expression patterns for *cmlc2* shown in K-M or for *ins* shown in N-P. (**K-M**) Expression of *cmlc2* in ~33 hpf embryos detected by in situ hybridization with antisense RNA probe. Scale bar, 150 μm. (**N-P**) Expression of *ins* in ~53 hpf embryos detected by in situ hybridization with antisense RNA probe. A dotted line marks the approximate midline. Scale bar: 150 μm.

position of the pancreas. In both cases, we observed randomized placement of the two organs in all of the above Arhgef11 loss-of-function scenarios. Whereas uninjected WT control embryos had heart fields localized on the left side, embryos deficient in Arhgef11 had randomized positioning of heart fields (Fig. 3J-M; Table 1). Moreover, in ΔDHPH-overexpressing embryos, many had two heart fields bilaterally located (data not shown).

The pancreas was typically observed on the right side of WT control embryos using the *ins* probe (Fig. 3J,N-P; Table 1). Following injection of either MO or the *Δdhph* construct, the pancreas was observed on the right side in a smaller percentage of the embryos, with many exhibiting medially-localized, or left-sided positioning. Additionally, in some ΔDHPH-overexpressing embryos, there were two separate bilateral fields of RNA expression (data not shown). Most *vu7/vu7* mutants failed to survive to 53 hpf, and therefore expression was not assayed in these embryos.

Given the left-right phenotypes observed in Arhgef11-deficient embryos, we assayed for disruption of structures that influence asymmetry. It has been proposed that proper midline development is important for establishing normal left-right asymmetries (Danos and Yost, 1996). In *arhgef11* morphants, the notochord and neural tube formed and the neural tube was patterned properly (Fig. 4A,B; see Fig. S3 in the supplementary material). However, these assays cannot completely exclude the possibility that a more subtle midline defect is present and contributes to the left-right defects in these embryos. In addition, endoderm and dorsal forerunners cells, which ultimately form Kupffer's vesicle (Cooper and D'Amico, 1996), appeared normal in morphants (see Fig. S2 in the supplementary material). Furthermore, the morphology of Kupffer's vesicle was comparable to that of uninjected WT control embryos and comprised ciliated cells (Fig. 4A-D). Cilia of MO^{SPL}-injected and *vu7/vu7* embryos were of normal length; however, cilia were significantly shortened after MO^{AUG}-injection (Fig. 4E).

Arhgef11 is necessary for formation of the normal number of ear otoliths

Since ciliated cells have multiple developmental roles in addition to affecting left-right asymmetry, we examined the effects on other processes that require ciliated epithelia in embryos with reduced Arhgef11 function. Ciliated cells of the developing ear are essential for proper formation of mineral-rich structures, called otoliths, which are important for its sensory functions (Riley et al., 1997; Popper and Lu, 2000). In mutants with defective cilia, such as *oval*, which harbors a mutation in the *polaris* gene, an excess number of otoliths is observed (Tsujikawa and Malicki, 2004). Likewise, whereas 98% (n=342) of WT control embryos had two otoliths and 2% had three, we observed three otoliths in 43% (n=252) of MO^{AUG}-injected embryos, with the remaining 43% and 14% having two or one otolith, respectively (Fig. 5A-C). Similarly, 49% (n=92) of embryos injected with MO^{SPL} had two otoliths and 51% had three. Among *vu7/vu7* mutants, 33% (n=99) had three otoliths and 67% had two. Finally, we also observed three otoliths in a small number (6%, n=66) of ΔDHPH-overexpressing embryos, with 83% having two otoliths and the remaining 11% one otolith.

Table 1. Expression of laterality markers after Arhgef11 loss-of-function

	Embryo type				
	WT	AUGMO	SPLMO	ΔDHPH	*vu7/vu7*
***spaw* in LPM (19 hpf)**					
n	513	194	92	306	64
L	88%	21%	50%	58%	75%
B	10%	5%	21%	15%	23%
R	2%	13%	25%	15%	0%
A	<1%	61%	4%	12%	2%
***pitx2* in LPM (21 hpf)**					
n	120	115	–	74	80
L	99%	35%	–	87%	85%
B	1%	14%	–	5%	10%
R	0%	29%	–	8%	0%
A	0%	22%	–	0%	5%
***cmlc2* (30 hpf)**					
n	220	96	106	65	173
L	99%	52%	79%	48%	78%
M	0%	23%	17%	14%	20%
R	<1%	25%	4%	0%	2%
T	0%	0%	0%	38%	0%
***ins* (53 hpf)**					
n	178	103	52	62	–
L	2%	29%	8%	8%	–
M	3%	21%	23%	11%	–
R	95%	50%	69%	73%	–
T	0%	0%	0%	8%	–

n, number of embryos; L, left-sided; B, bilateral; R, right-sided; A, absent; M, medial; T, two fields.

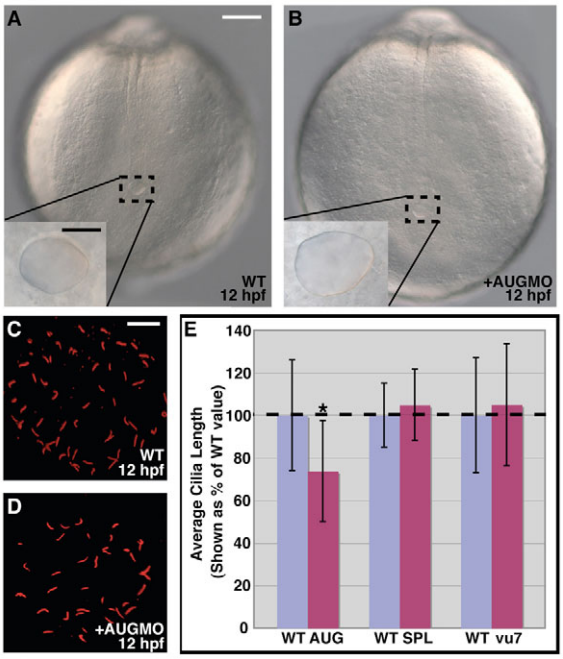

Fig. 4. Arhgef11 is not required for formation of Kupffer's vesicle and cilia. (**A**,**B**) Posterior region of live, uninjected WT and MO-injected embryos. The inset is a magnified view of Kupffer's vesicle. White scale bar, 100 μm; black scale bar, 25 μm. (**C**,**D**) Acetylated tubulin immunostaining of cilia within Kupffer's vesicle. Scale bar, 10 μm. (**E**) Comparison of Kupffer's vesicle cilia length for WT control, MO-injected (AUG, SPL) and *vu7/vu7* embryos. The asterisk marks significantly different lengths ($P \leqslant 0.001$).

Proper development of the pronephros requires Arhgef11

We next examined the developing pronephros, which includes pronephric ducts comprising both mono- and multi-ciliated epithelial cells. In many mutants with abnormal cilia, fluid-filled cysts develop within these ducts (Otto et al., 2003; Sun et al., 2004; Kramer-Zucker et al., 2005). As mentioned above, both protein and RNA encoding Arhgef11 were found in the pronephric ducts of uninjected WT embryos at 24 hpf (Fig. 1E′, Fig. 6A). Notably, Arhgef11 protein was enriched in apical regions of these cells, whereas it was reduced or absent in embryos injected with MO^{AUG} and in *vu7/vu7* mutants (Fig. 6A,A′ and data not shown). We also observed considerable distention of the pronephric ducts in live morphants at 24 hpf and later. Indeed, cross-sections of morphant embryos after 54 hpf showed the presence of cysts within the pronephric ducts (Fig. 6E-G), and these cysts became morphologically apparent by 80 hpf (Fig. 6H,I). However, anti-acetylated tubulin staining revealed that cilia were still present in Arhgef11 morphants (Fig. 6C,C′). In addition, we monitored the ability of these cilia to beat in morphant pronephric ducts using high-speed video imaging. Cilia within cystic morphant ducts appeared to beat at rates similar to, or slightly faster than, those in uninjected control embryos (see Movies 1, 2 in the supplementary material). Additionally, as in WT embryos, both mono- and multi-ciliated cells were observed in the pronephric ducts of Arhgef11 morphants.

We next asked whether apical-basal polarity was otherwise affected in the cells of the pronephric ducts after interference with Arhgef11. We used immunohistochemistry on cryosections of control and MO^{AUG}-injected embryos to assay the localization of proteins known to be distributed on the apical or basal side of these polarized cells. The tight-junction marker Zona Occludins 1 (ZO1; Tjp1 – Zebrafish Information Network) and atypical Protein kinase C (aPKCζ; Prkci – Zebrafish Information Network) were localized to the apical side of the pronephric ducts in uninjected WT and morphant embryos (Fig. 7C,D). Localization of the microtubule-

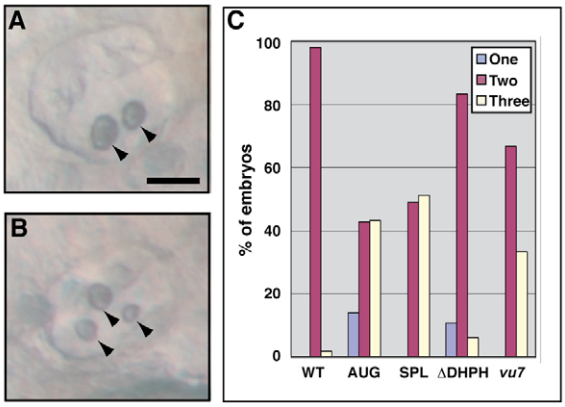

Fig. 5. Arhgef11 function is important for proper otolith development. (**A**,**B**) Otic vesicles of example embryos at ~48 hpf showing two or three otoliths (arrowheads). Scale bar, 50 μm. (**C**) Bar graph of the percentage of WT control, MO-injected, ΔDHPH-overexpressing, and mutant embryos with two otoliths in both otic vesicles, or with an abnormal number (one or three) in at least one otic vesicle.

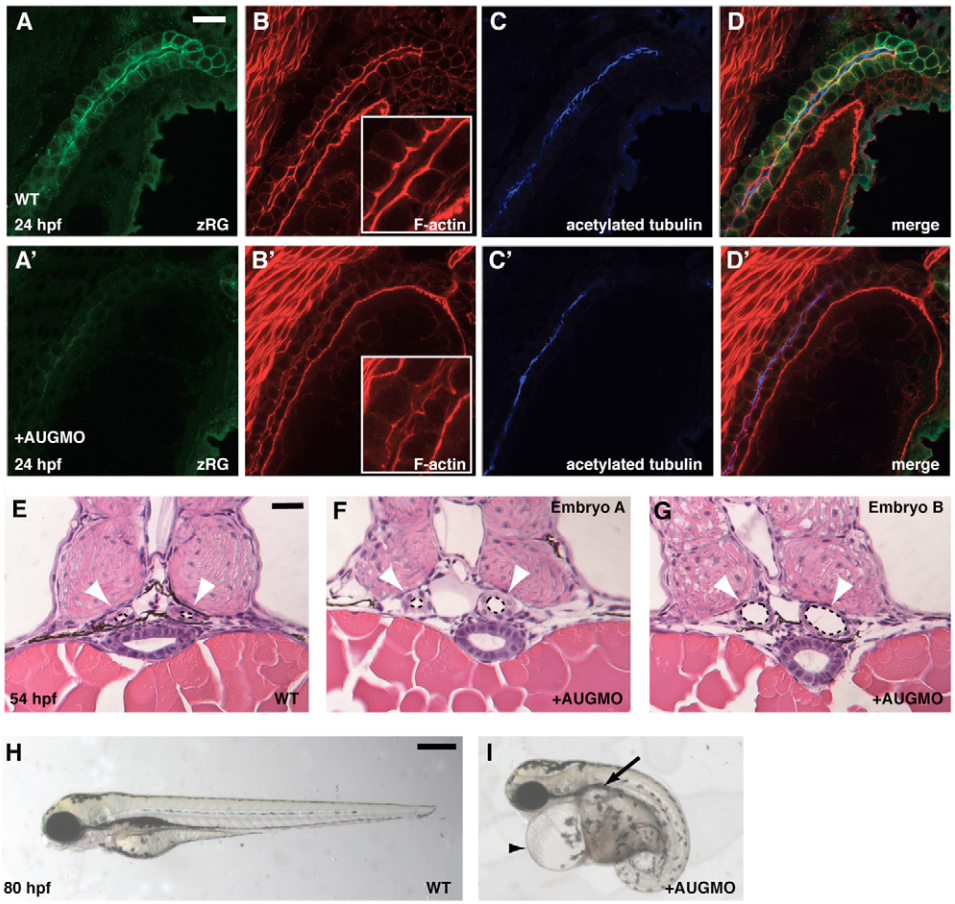

Fig. 6. Loss of Arhgef11 function leads to formation of pronephric cysts. (**A-D'**) Fluorescent immunostaining of 24 hpf WT control and MO^{AUG}-injected embryos to visualize zRG (green), F-actin (red) with magnified view inset, and acetylated tubulin (blue). Scale bar, 20 μm. (**E-G**) JB-4 sections of 54 hpf WT control embryos (E) compared with sections from two embryos injected with 4 ng MO^{AUG} (F,G) at the same stage. Pronephric ducts are indicated by white arrowheads, and their lumens are outlined by dotted lines. Scale bar, 25 μm. (**H**,**I**) Live embryos at 80 hpf showing an uninjected WT embryo (H) compared with WT injected with 4 ng MO^{AUG} (I), which exhibits cardiac edema (arrowhead) and pronephric cysts (arrow). Scale bar: 300 μm.

organizing center, as visualized by gamma-tubulin antibody, was also apically-localized in both control and morphant embryos (Fig. 7E,F).

Since modulation of Rho signaling can lead to changes in the actin cytoskeleton, and given that the human ARHGEF11 has been shown to interact with actin (Banerjee and Wedegaertner, 2004), we hypothesized that Arhgef11-deficient embryos would have a disrupted actin organization. We visualized the distribution of filamentous actin in the pronephric ducts using phalloidin. As in control embryos, morphants showed an enrichment of actin at the apical side of these cells, but it appeared slightly less organized (Fig. 6B,B′; Fig. 7A,B). Notably, Na^+/K^+-ATPase, an ion channel localized baso-laterally in the pronephric ducts of uninjected WT embryos (Drummond et al., 1998) (Fig. 7G), was reduced and frequently absent from the basal regions of the cells in morphant embryos (Fig. 7H). Taken together, these experiments indicate that interference with *arhgef11* function does not completely eradicate the apical-basal polarity of pronephric duct cells, but causes mislocalization of certain proteins. Thus, we propose that such defective intracellular protein distribution in pronephric ducts could underlie their abnormal function in Arhgef11-deficient embryos.

DISCUSSION

In this study, we have endeavored to elucidate the roles of Arhgef11 in the developing vertebrate embryo. We showed through mapping and cell culture experiments that Arhgef11 is a zebrafish homolog of human ARHGEF11, with the ability to remodel the actin cytoskeleton. In addition, through several loss-of-function approaches, we demonstrated that Arhgef11 is required for multiple developmental processes that involve ciliated epithelia, including establishment of left-right asymmetry and proper development of otoliths and the pronephros. We have uncovered important new roles for Arhgef11, which were unanticipated by studies of this molecule in the fruit fly and mammalian cell culture. These functions are likely to extend to other vertebrates.

The large number of exons in *arhgef11* in zebrafish and mammals provides ample opportunity for alternative splicing events to produce different transcripts and modulate the function of the resulting protein. We have detected two alternative splice forms of *arhgef11* expressed during early fish development. Interestingly, the alternatively-spliced exon encoding amino acids 556-566 of the zebrafish protein corresponds to an exon of the same length encoding human ARHGEF11 that was also reported to undergo an alternative splicing event (Hart et al., 2000), and 9 of the 11 amino

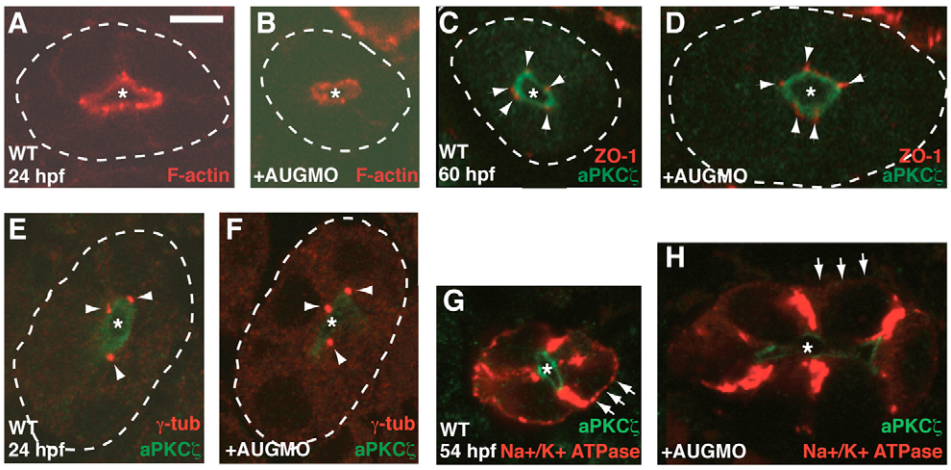

Fig. 7. Apical-basal distribution of Na^+/K^+-ATPase is disrupted in morphants. Cryosections through pronephric ducts of uninjected WT (**A**,**C**,**E**,**G**) and MO^{AUG}-injected (**B**,**D**,**F**,**H**) embryos at the indicated developmental times. The lumen (apical) is indicated by an asterisk, and the basal sides of ducts are outlined by dotted lines in A-F. (A,B) Filamentous actin in the pronephric ducts (red). (C,D) Cell junctions are stained with ZO1 antibody (red, arrowheads), and the apical region of the cells is marked by aPKCζ (green). (E,F) Microtubule-organizing centers are stained with anti-γ-tubulin (red, arrowheads), and the apical region of the cells is marked by aPKCζ (green). (G,H) Localization of Na^+/K^+-ATPase (red); the apical region of the cells is marked by aPKCζ (green). Arrows highlight the presence of staining in basal regions of WT control cells and its absence in morphants. Scale bar: 5 μm.

acids are identical. Conservation of this alternative splicing and the location of this exon near a region that mediates the interaction of ARHGEF11 with actin (Banerjee and Wedegaertner, 2004), suggest that splicing events may be important for regulating this interaction. As mentioned above, the C-terminus of the human homolog associates with p-21 activated kinase 4 (Barac et al., 2004), and is important for homo- and heterodimerization with ARHGEF11 and ARHGEF12 molecules, respectively (Chikumi et al., 2004). We predict that modification through alternative splicing of the exon encoding amino acids 1232-1257 could affect this or other important interactions.

Our studies revealed RNA and protein expression throughout embryogenesis, being particularly enriched in the pronephric ducts, suggesting that Arhgef11 plays a role during early development. Indeed, injection of MOs designed to interfere with either translation or splicing of *arhgef11* led to developmental abnormalities characterized by a ventrally-curved body, enlarged brain ventricles, and defects in laterality, otolith formation and the pronephric ducts, whereas the other loss-of-function approaches yielded somewhat milder, yet similar defects. The different loss-of-function approaches were expected to produce overlapping but slightly different phenotypes. First, the weaker laterality defects observed with MO^{SPL} and *vu7/vu7* are likely to be due to maternally-deposited RNA or protein (Fig. 1 and data not shown), as these would not be diminished in either situation, whereas translation of maternal RNA would be affected by MO^{AUG}. As discussed above, the dominant-negative form acts to competitively inhibit Arhgef11 function by binding to upstream signals without generating activated Rho (Fukuhara et al., 1999; Rumenapp et al., 1999). One would predict expression of this form to yield a somewhat weaker defect than the MOs, as the endogenous full-length form is not eliminated by this method and may still achieve some level of Rho activation. Indeed, we did observe defects in left-right asymmetry and otolith formation, similar to those detected in morphants. The major differences we noted between these and morpholino-injected embryos were two expression domains of *cmlc2* and *ins*, cardia bifida, and the absence of a ventral curve. Since cardia bifida was not observed in the morphants or the *vu7/vu7* mutants, we attribute this phenotype to interference with the function of a similar RhoGEF, such as Arhgef12, which interacts with many of the same molecules as ARHGEF11 via its PDZ and RGS domains (Fukuhara et al., 2001; Swiercz et al., 2002). Interestingly, previous work using the chick embryo showed defects in left-right asymmetry and cardia bifida after inhibition of Rho kinase, a downstream effector of Rho (Wei et al., 2001). Inhibition of Rho kinase or Rho in zebrafish impairs gastrulation movements (Marlow et al., 2002; Zhu et al., 2006) and causes cardia bifida (Matsui et al., 2005), consistent with involvement of RhoGEFs in midline convergence of heart precursors.

Since all the laterality markers we examined were affected to some degree by loss of Arhgef11 activity, we conclude that it functions upstream of these genes in an early step to establish left-right asymmetry, possibly by regulating the ciliated cells that constitute Kupffer's vesicle. The fact that loss of function also leads to defects in other processes involving ciliated epithelia, such as the formation of otoliths in the otic vesicles and proper development of the pronephric ducts, supports the notion that Arhgef11 plays an important role in the cells of these structures. This is an unexpected finding because we anticipated defects similar to those in the *D. melanogaster* RhoGEF2 mutants, where loss of function disrupted gastrulation cell movements and epithelial folding (Barrett et al., 1997; Hacker and Perrimon, 1998; Nikolaidou and Barrett, 2004; Padash Barmchi et al., 2005). Many recent reports point to cilia as important components in an increasing number of processes, but their formation and ability to beat appear largely unaffected in Arghef11-deficient embryos. In addition to the aforementioned roles, these structures are also implicated in Hedgehog signaling and growth control in mammalian embryos (Corbit et al., 2005; Huangfu and Anderson, 2005; Schneider et al., 2005). By contrast, our examination of Hedgehog-dependent cell types and gene expression in embryos after Arhgef11 loss-of-function did not reveal any defects (see Fig. S3 in the supplementary material). However, we cannot completely rule out a role for zebrafish Arhgef11 in cilia formation and function because a reduction in cilia length correlates with our strongest loss-of-function phenotypes.

In the case of the pronephric ducts, these tubular structures contain ciliated epithelial cells. The apical side of the cells faces the lumen and the cell junctions are important for maintaining its structural integrity and to serve as a selectively-permeable barrier to water and solutes. Examination of the cilia and apical-basal polarity of the renal epithelial cells did not reveal any obvious defects in localization of most polarized proteins, with the exception of Na^+/K^+-ATPase, the basal expression of which was lost in morphants. Indeed, the distribution of this protein was often disrupted in other zebrafish kidney mutants where cysts developed (Drummond et al., 1998). Whether this mislocalization is directly or indirectly due to Arhgef11 loss-of-function remains to be determined, but given its known functions, the mechanism is likely to be through modulation of the cytoskeleton. Accordingly, our data also hint that apical actin structures are slightly misorganized in morphants. Since Na^+/K^+-ATPase is important for maintaining the ionic gradient and the osmotic balance in these cells (Drummond, 2000; Rajasekaran et al., 2005), incorrect positioning in morphants, as a result of cytoskeletal disruption, could account for impaired pronephric function. Interestingly, recent work with RhoGEF2 demonstrated that this protein stimulates Rho and, subsequently, actin remodeling in apical regions of epithelial cells within the fruit fly embryo so as to modulate invagination and lumen maintenance of the tubular structures called spiracles (Simoes et al., 2006). It is plausible that the zebrafish homolog functions similarly to maintain the epithelial structures affected in our experiments. Since this study has not exhaustively examined the cilia of the pronephric ducts, the possibility remains that some other aspect of the cilia are affected in Arhgef11-deficient embryos, such as coordination of beating and anchoring of the basal body, thereby leading to cyst formation.

Although the exact mechanism by which Arhgef11 affects ciliated epithelia remains unclear, its mere involvement opens up a wide range of possible pathways that could also play a role here. For the pronephric ducts, this seems to be a highly specialized RhoGEF, where its expression is transcriptionally-regulated and its localization is enriched to the apical side of the cell. With its multiple functional domains and the many interactions identified in other systems, this RhoGEF could prove a very interesting protein, possibly linking Plexins or G protein-coupled signaling to cytoskeletal modification of ciliated and other highly polarized cells in vivo. Interestingly, RhoGEF2 is enriched on the apical surface of epithelial cells during development in *D. melanogaster* (Padash Barmchi et al., 2005). We hypothesize that there may be some similar roles for Arhgef11 and its invertebrate homolog, but as ciliated epithelia are unique to vertebrates, so might be these new functions that we have uncovered for Arhgef11.

We thank members of the L.S.-K., J. Gamse, C. Wright, E. Knapik, T. Zhong, B. Appel and P. Bock laboratories for reagents and discussion; Yan Liu for help conducting cilia movement analysis; and Joshua Clanton and Amanda Bradshaw for excellent technical assistance. This work was supported by NIH grant 2T32HD07502, NIH grant GM77770 (to L.S.-K.), and NIH grant DK53093 (to I.A.D.).

Supplementary material

Supplementary material for this article is available at http://dev.biologists.org/cgi/content/full/134/5/921/DC1

References

Aurandt, J., Vikis, H. G., Gutkind, J. S., Ahn, N. and Guan, K. L. (2002). The semaphorin receptor plexin-B1 signals through a direct interaction with the Rho-specific nucleotide exchange factor, LARG. *Proc. Natl. Acad. Sci. USA* **99**, 12085-12090.

Banerjee, J. and Wedegaertner, P. B. (2004). Identification of a novel sequence in PDZ-RhoGEF that mediates interaction with the actin cytoskeleton. *Mol. Biol. Cell* **15**, 1760-1775.

Barac, A., Basile, J., Vazquez-Prado, J., Gao, Y., Zheng, Y. and Gutkind, J. S. (2004). Direct interaction of p21-activated kinase 4 with PDZ-RhoGEF, a G protein-linked Rho guanine exchange factor. *J. Biol. Chem.* **279**, 6182-6189.

Barrett, K., Leptin, M. and Settleman, J. (1997). The Rho GTPase and a putative RhoGEF mediate a signaling pathway for the cell shape changes in Drosophila gastrulation. *Cell* **91**, 905-915.

Bisgrove, B. W., Snarr, B. S., Emrazian, A. and Yost, H. J. (2005). Polaris and Polycystin-2 in dorsal forerunner cells and Kupffer's vesicle are required for specification of the zebrafish left-right axis. *Dev. Biol.* **287**, 274-288.

Cerione, R. A. and Zheng, Y. (1996). The Dbl family of oncogenes. *Curr. Opin. Cell Biol.* **8**, 216-222.

Chikumi, H., Barac, A., Behbahani, B., Gao, Y., Teramoto, H., Zheng, Y. and Gutkind, J. S. (2004). Homo- and hetero-oligomerization of PDZ-RhoGEF, LARG and p115RhoGEF by their C-terminal region regulates their in vivo Rho GEF activity and transforming potential. *Oncogene* **23**, 233-240.

Cooper, M. S. and D'Amico, L. A. (1996). A cluster of noninvoluting endocytic cells at the margin of the zebrafish blastoderm marks the site of embryonic shield formation. *Dev. Biol.* **180**, 184-198.

Corbit, K. C., Aanstad, P., Singla, V., Norman, A. R., Stainier, D. Y. and Reiter, J. F. (2005). Vertebrate Smoothened functions at the primary cilium. *Nature* **437**, 1018-1021.

Danos, M. C. and Yost, H. J. (1996). Role of notochord in specification of cardiac left-right orientation in zebrafish and Xenopus. *Dev. Biol.* **177**, 96-103.

Drummond, I. A. (2000). The zebrafish pronephros: a genetic system for studies of kidney development. *Pediatr. Nephrol.* **14**, 428-435.

Drummond, I. A., Majumdar, A., Hentschel, H., Elger, M., Solnica-Krezel, L., Schier, A. F., Neuhauss, S. C., Stemple, D. L., Zwartkruis, F., Rangini, Z. et al. (1998). Early development of the zebrafish pronephros and analysis of mutations affecting pronephric function. *Development* **125**, 4655-4667.

Essner, J. J., Amack, J. D., Nyholm, M. K., Harris, E. B. and Yost, H. J. (2005). Kupffer's vesicle is a ciliated organ of asymmetry in the zebrafish embryo that initiates left-right development of the brain, heart and gut. *Development* **132**, 1247-1260.

Fukuhara, S., Murga, C., Zohar, M., Igishi, T. and Gutkind, J. S. (1999). A novel PDZ domain containing guanine nucleotide exchange factor links heterotrimeric G proteins to Rho. *J. Biol. Chem.* **274**, 5868-5879.

Fukuhara, S., Chikumi, H. and Gutkind, J. S. (2001). RGS-containing RhoGEFs: the missing link between transforming G proteins and Rho? *Oncogene* **20**, 1661-1668.

Hacker, U. and Perrimon, N. (1998). DRhoGEF2 encodes a member of the Dbl family of oncogenes and controls cell shape changes during gastrulation in Drosophila. *Genes Dev.* **12**, 274-284.

Hart, M. J., Roscoe, W. and Bollag, G. (2000). Activation of Rho GEF activity by G alpha 13. *Meth. Enzymol.* **325**, 61-71.

Huangfu, D. and Anderson, K. V. (2005). Cilia and Hedgehog responsiveness in the mouse. *Proc. Natl. Acad. Sci. USA* **102**, 11325-11330.

Hubbard, T., Andrews, D., Caccamo, M., Cameron, G., Chen, Y., Clamp, M., Clarke, L., Coates, G., Cox, T., Cunningham, F. et al. (2005). Ensembl 2005. *Nucleic Acids Res.* **33**, D447-D453.

Iwamoto, H., Blakely, R. D. and De Felice, L. J. (2006). Na^+, Cl^-, and pH dependence of the human choline transporter (hCHT) in Xenopus oocytes: the proton inactivation hypothesis of hCHT in synaptic vesicles. *J. Neurosci.* **26**, 9851-9859.

Jessen, J. R., Topczewski, J., Bingham, S., Sepich, D. S., Marlow, F., Chandrasekhar, A. and Solnica-Krezel, L. (2002). Zebrafish trilobite identifies new roles for Strabismus in gastrulation and neuronal movements. *Nat. Cell Biol.* **4**, 610-615.

Kane, D. A. and Kimmel, C. B. (1993). The zebrafish midblastula transition. *Development* **119**, 447-456.

Kimmel, C. B., Ballard, W. W., Kimmel, S. R., Ullmann, B. and Schilling, T. F. (1995). Stages of embryonic development of the zebrafish. *Dev. Dyn.* **203**, 253-310.

Kramer-Zucker, A. G., Olale, F., Haycraft, C. J., Yoder, B. K., Schier, A. F. and Drummond, I. A. (2005). Cilia-driven fluid flow in the zebrafish pronephros, brain and Kupffer's vesicle is required for normal organogenesis. *Development* **132**, 1907-1921.

Kuner, R., Swiercz, J. M., Zywietz, A., Tappe, A. and Offermanns, S. (2002). Characterization of the expression of PDZ-RhoGEF, LARG and G(alpha)12/G(alpha)13 proteins in the murine nervous system. *Eur. J. Neurosci.* **16**, 2333-2341.

Laemmli, U. K. (1970). Cleavage of structural proteins during the assembly of the head of bacteriophage T4. *Nature* **227**, 680-685.

Levin, M. (2005). Left-right asymmetry in embryonic development: a comprehensive review. *Mech. Dev.* **122**, 3-25.

Long, S., Ahmad, N. and Rebagliati, M. (2003). The zebrafish nodal-related gene southpaw is required for visceral and diencephalic left-right asymmetry. *Development* **130**, 2303-2316.

Marlow, F., Zwartkruis, F., Malicki, J., Neuhauss, S. C., Abbas, L., Weaver, M., Driever, W. and Solnica-Krezel, L. (1998). Functional interactions of genes

mediating convergent extension, knypek and trilobite, during the partitioning of the eye primordium in zebrafish. *Dev. Biol.* **203**, 382-399.
Marlow, F., Topczewski, J., Sepich, D. and Solnica-Krezel, L. (2002). Zebrafish Rho kinase 2 acts downstream of Wnt11 to mediate cell polarity and effective convergence and extension movements. *Curr. Biol.* **12**, 876-884.
Matsui, T., Raya, A., Kawakami, Y., Callol-Massot, C., Capdevila, J., Rodriguez-Esteban, C. and Izpisua Belmonte, J. C. (2005). Noncanonical Wnt signaling regulates midline convergence of organ primordia during zebrafish development. *Genes Dev.* **19**, 164-175.
Milewski, W. M., Duguay, S. J., Chan, S. J. and Steiner, D. F. (1998). Conservation of PDX-1 structure, function, and expression in zebrafish. *Endocrinology* **139**, 1440-1449.
Murphy, J. T., Duffy, S. L., Hybki, D. L. and Kamm, K. (2001). Thrombin-mediated permeability of human microvascular pulmonary endothelial cells is calcium dependent. *J. Trauma* **50**, 213-222.
Nagase, T., Ishikawa, K., Nakajima, D., Ohira, M., Seki, N., Miyajima, N., Tanaka, A., Kotani, H., Nomura, N. and Ohara, O. (1997). Prediction of the coding sequences of unidentified human genes. VII. The complete sequences of 100 new cDNA clones from brain which can code for large proteins in vitro. *DNA Res.* **4**, 141-150.
Nasevicius, A. and Ekker, S. C. (2000). Effective targeted gene 'knockdown' in zebrafish. *Nat. Genet.* **26**, 216-220.
Nikolaidou, K. K. and Barrett, K. (2004). A Rho GTPase signaling pathway is used reiteratively in epithelial folding and potentially selects the outcome of Rho activation. *Curr. Biol.* **14**, 1822-1826.
Oleksy, A., Opalinski, L., Derewenda, U., Derewenda, Z. S. and Otlewski, J. (2006). The molecular basis of RhoA specificity in the guanine nucleotide exchange factor PDZ-RhoGEF. *J. Biol. Chem.* **281**, 32891-32897.
Otto, E. A., Schermer, B., Obara, T., O'Toole, J. F., Hiller, K. S., Mueller, A. M., Ruf, R. G., Hoefele, J., Beekmann, F., Landau, D. et al. (2003). Mutations in INVS encoding inversin cause nephronophthisis type 2, linking renal cystic disease to the function of primary cilia and left-right axis determination. *Nat. Genet.* **34**, 413-420.
Padash Barmchi, M., Rogers, S. and Hacker, U. (2005). DRhoGEF2 regulates actin organization and contractility in the Drosophila blastoderm embryo. *J. Cell Biol.* **168**, 575-585.
Panizzi, P., Boxrud, P. D., Verhamme, I. M. and Bock, P. E. (2006). Binding of the COOH-terminal lysine residue of streptokinase to plasmin(ogen) kringles enhances formation of the streptokinase.plasmin(ogen) catalytic complexes. *J. Biol. Chem.* **281**, 26774-26778.
Perrot, V., Vazquez-Prado, J. and Gutkind, J. S. (2002). Plexin B regulates Rho through the guanine nucleotide exchange factors leukemia-associated Rho GEF (LARG) and PDZ-RhoGEF. *J. Biol. Chem.* **277**, 43115-43120.
Popper, A. N. and Lu, Z. (2000). Structure-function relationships in fish otolith organs. *Fish. Res.* **46**, 15-25.
Rajasekaran, S. A., Barwe, S. P. and Rajasekaran, A. K. (2005). Multiple functions of Na,K-ATPase in epithelial cells. *Semin. Nephrol.* **25**, 328-334.
Riley, B. B., Zhu, C., Janetopoulos, C. and Aufderheide, K. J. (1997). A critical period of ear development controlled by distinct populations of ciliated cells in the zebrafish. *Dev. Biol.* **191**, 191-201.
Rogers, S. L., Wiedemann, U., Hacker, U., Turck, C. and Vale, R. D. (2004). Drosophila RhoGEF2 associates with microtubule plus ends in an EB1-dependent manner. *Curr. Biol.* **14**, 1827-1833.
Rossman, K. L., Der, C. J. and Sondek, J. (2005). GEF means go: turning on RHO GTPases with guanine nucleotide-exchange factors. *Nat. Rev. Mol. Cell Biol.* **6**, 167-180.
Rumenapp, U., Blomquist, A., Schworer, G., Schablowski, H., Psoma, A. and Jakobs, K. H. (1999). Rho-specific binding and guanine nucleotide exchange catalysis by KIAA0380, a dbl family member. *FEBS Lett.* **459**, 313-318.
Rupp, R. A., Snider, L. and Weintraub, H. (1994). Xenopus embryos regulate the nuclear localization of XMyoD. *Genes Dev.* **8**, 1311-1323.
Schmidt, A. and Hall, A. (2002). Guanine nucleotide exchange factors for Rho GTPases: turning on the switch. *Genes Dev.* **16**, 1587-1609.
Schneider, L., Clement, C. A., Teilmann, S. C., Pazour, G. J., Hoffmann, E. K., Satir, P. and Christensen, S. T. (2005). PDGFRalphaalpha signaling is regulated through the primary cilium in fibroblasts. *Curr. Biol.* **15**, 1861-1866.
Simoes, S., Denholm, B., Azevedo, D., Sotillos, S., Martin, P., Skaer, H., Hombria, J. C. and Jacinto, A. (2006). Compartmentalisation of Rho regulators directs cell invagination during tissue morphogenesis. *Development* **133**, 4257-4267.
Solnica-Krezel, L., Schier, A. F. and Driever, W. (1994). Efficient recovery of ENU-induced mutations from the zebrafish germline. *Genetics* **136**, 1401-1420.
Sun, Z., Amsterdam, A., Pazour, G. J., Cole, D. G., Miller, M. S. and Hopkins, N. (2004). A genetic screen in zebrafish identifies cilia genes as a principal cause of cystic kidney. *Development* **131**, 4085-4093.
Swiercz, J. M., Kuner, R., Behrens, J. and Offermanns, S. (2002). Plexin-B1 directly interacts with PDZ-RhoGEF/LARG to regulate RhoA and growth cone morphology. *Neuron* **35**, 51-63.
Tatusova, T. A. and Madden, T. L. (1999). BLAST 2 Sequences, a new tool for comparing protein and nucleotide sequences. *FEMS Microbiol. Lett.* **174**, 247-250.
Thisse, C. and Thisse, B. (1998). High resolution whole-mount *in situ* hybridization. *Zebrafish Science Monitor* **5**, 8-9.
Topczewska, J. M., Topczewski, J., Shostak, A., Kume, T., Solnica-Krezel, L. and Hogan, B. L. (2001). The winged helix transcription factor Foxc1a is essential for somitogenesis in zebrafish. *Genes Dev.* **15**, 2483-2493.
Tsujikawa, M. and Malicki, J. (2004). Intraflagellar transport genes are essential for differentiation and survival of vertebrate sensory neurons. *Neuron* **42**, 703-716.
Tsukui, T., Capdevila, J., Tamura, K., Ruiz-Lozano, P., Rodriguez-Esteban, C., Yonei-Tamura, S., Magallon, J., Chandraratna, R. A., Chien, K., Blumberg, B. et al. (1999). Multiple left-right asymmetry defects in Shh(–/–) mutant mice unveil a convergence of the shh and retinoic acid pathways in the control of Lefty-1. *Proc. Natl. Acad. Sci. USA* **96**, 11376-11381.
Wei, L., Roberts, W., Wang, L., Yamada, M., Zhang, S., Zhao, Z., Rivkees, S. A., Schwartz, R. J. and Imanaka-Yoshida, K. (2001). Rho kinases play an obligatory role in vertebrate embryonic organogenesis. *Development* **128**, 2953-2962.
Yelon, D., Horne, S. A. and Stainier, D. Y. (1999). Restricted expression of cardiac myosin genes reveals regulated aspects of heart tube assembly in zebrafish. *Dev. Biol.* **214**, 23-37.
Zhu, S., Liu, L., Korzh, V., Gong, Z. and Low, B. C. (2006). RhoA acts downstream of Wnt5 and Wnt11 to regulate convergence and extension movements by involving effectors Rho kinase and Diaphanous: use of zebrafish as an in vivo model for GTPase signaling. *Cell. Signal.* **18**, 359-372.